SYSTEM IDENTIFICATION OF PIEZOCERAMIC BEAMS

Rong-Liang Chen
Bor-Tsuen Wang

Department of Mechanical Engineering
National Pingtung University of Science and Technology
Pingtung, Taiwan 91207
Republic of China

ABSTRACT

This paper presents the system identification technique by applying PZT actuators and PVDF sensors. An array of finite-length PVDF films is equally spaced and distributed over a cantilever beam acting as sensors. Two finite-length PZT patches are bonded symmetrically and excited 180° out-of-phase for pure bending excitation. The theoretical base of modal analysis for system identification of piezoceramic beams is presented to derive the frequency response functions (FRFs) in conventional modal format. The physical interpretation of PZT and PVDF mode shape functions are characterized respectively. The FRFs between the PZT actuators and PVDF sensors are experimentally measured. By the operation of a series of FRFs and the application of modal parameter extraction method, the modal parameters, including system natural frequencies, mode shapes and modal damping ratios, can be obtained. Both theoretical and experimental approaches agree very well. The system information can be used for control applications and also be applicable to structural failure diagnosis.

INTRODUCTION

The PZT actuator and PVDF sensors have been widely applied in active structural vibration and acoustic control. The PZT patches can be arranged symmetrically for pure bending excitation for beams [1-3] and plates [4,5] or asymmetric excitation [6]. The PVDF films can be cut as a rectangular patch or a strip applied to the structure as sensing devices [7,8]. Particular shapes of PVDF films can also be formed to act as modal sensors for beams [9] and plates [10]. Previous work [11] has theoretically verified the feasibility of using piezoceramic transducers for cantilever beam modal testing. An array of finite-length PVDF films can be equally spaced and distributed over the beam acting as sensors. Wang and Wang [11] identified the PZT and PVDF mode shape functions to be proportional to the mode shapes of slope difference between the two edges of PZT and PVDF patches. This paper will experimentally identify the system modal parameters of the piezoceramic beam.

THEORETICAL ANALYSIS

A brief review of theoretical analysis for cantilever beam analysis is summarized as follows [11]. From the free vibration analysis, the natural frequencies can be determined and the corresponding mode shape functions are identified as follows:

$$\omega_n = (\alpha_n L_b)^2 \sqrt{\frac{E_b I_b}{\rho_b b_b t_b L_b^4}} = \alpha_n^2 \sqrt{\frac{E_b I_b}{\rho_b b_b t_b}} \tag{1}$$

$$\phi_n(x) = \cosh\alpha_n x - \cos\alpha_n x - \sigma_n(\sinh\alpha_n x - \sin\alpha_n x) \tag{2}$$

where

$$\sigma_n = \frac{\sinh\alpha_n L_b - \sin\alpha_n L_b}{\cosh\alpha_n L_b + \cos\alpha_n L_b} \tag{3}$$

It is noted that $\phi_n(x)$ is a continuous function and represents the displacement mode shape.

Consider the j-the PZT patches be symmetrically bonded on the top and the bottom of the beam and applied voltage V_{c_j} 180^0 out-of-phase as shown in Figure 1. The equivalent force induced by the PZT patches can be shown as two concentrated moments at both edges of the PZT patches. A strip of PVDF patch can also be applied as the sensing device as shown in Figure 1. The FRF between the measured voltage of the i-th PVDF sensor, V_{p_i}, and the voltage amplitude applied by the PZT actuator, V_{c_j}, can be Obtained as follows:

$$\alpha_{p_i c_j} = \frac{V_{P_i}}{V_{C_j}} = -\omega^2 \sum_{n=1}^{\infty} \frac{{}_i\Phi_n^p \, {}_j\Phi_n^c}{\rho_b b_b t_b[(\omega_n^2 - \omega^2) + i2\xi_n\omega_n\omega]} \tag{4}$$

where

$${}_i\Phi_n^p = \sqrt{\frac{1}{L_b}} k_p \left[\phi_n'(x_{p_i} + l_p/2) - \phi_n'(x_{p_i} - l_p/2)\right],$$

$$k_p = \frac{t_p}{\varepsilon A_p} \frac{t_b + t_p}{2} b_p e_{31} \tag{5}$$

$${}_j\Phi_n^c = \sqrt{\frac{1}{L_b}} k_c \left[\phi_n'(x_{c_i} + l_c/2) - \phi_n'(x_{c_i} - l_c/2)\right],$$

$$k_c = \frac{C_0 d_{31}}{t_c} \tag{6}$$

$$\phi_n'(x) = \alpha_n\{\cosh\alpha_n x - \cos\alpha_n x - \sigma_n(\sinh\alpha_n x - \sin\alpha_n x)\} \tag{7}$$

${}_i\Phi_n^p$ and ${}_j\Phi_n^c$ represent the values of the n-th PVDF and PZT mode shape functions at the i-th and j-th location of the PVDF sensor and PZT actuator respectively. The PVDF and PZT mode shape functions are proportional to the mode shape of the slope difference between the two edges of PVDF and PZT patches and can be shown to be the mirror image of displacement mode shapes against the clamped end.

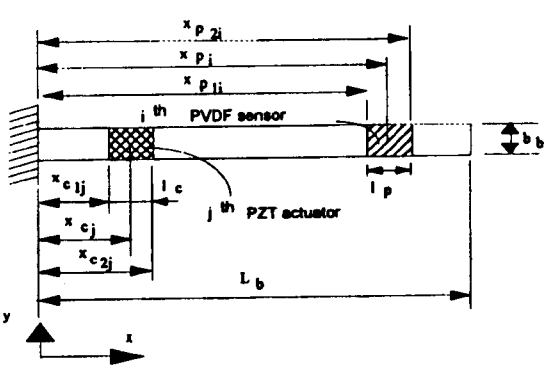

Figure 1. System arrangement of coordinates

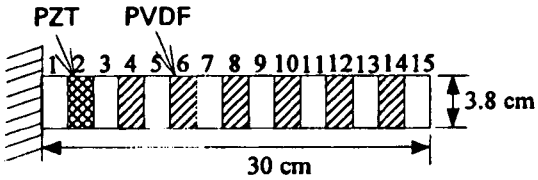

Figure 2. Division and numbering of cantilever beam

It should be noted that in practical measurement a continuous structure is always discretized, and so forth only a finite number of points N can be measured. The NxN FRF matrix can then be measured through the mobility measurement. The FRF matrix $[\alpha_{ij}]$ can be defined as follows:

$$\{z_i\}_{Nx1} = [\alpha_{ij}]_{NxN} \{p_j\}_{Nx1} \quad (8)$$

where $\{z_i\}_{Nx1}$ and $\{p_j\}_{Nx1}$ represents the output and input vectors respectively. The component of FRF matrix is shown in Equation (4) which are written in the conventional FRF format.

To perform experimental modal analysis, at least, either a row or a column of FRF matrix must be measured. By roving the actuator, a row of FRF matrix can be obtained; and by roving the sensor, a column of FRF matrix will be obtained. In summary, when the sensor is roving with the actuator fixed during testing, a column of FRF matrix can be determined. The extracted mode shape will then be characterized by the sensor mode shape. Conversely, when the actuator is roving with the sensor fixed, a row of FRF matrix can be obtained. The extracted mode shape will then be characterized by the actuator mode shape. In this work, the PZT actuator is fixed, and the PVDF sensor is roving; therefore, a column of FRF matrix can be obtained. The extracted mode shapes will then be the PVDF sensor mode shapes.

EXPERIMENTAL SETUP AND PROCEDURES

This work applies the piezoceramic transducers, i.e., the PZT actuator and PVDF sensors as arranged and shown in Figure 2, to perform structural modal testing in the replacement of conventional transducers. The experimental setup is shown in Figure 3. The BK3550 is a two-channel FFT analyzer. The pure bending PZT actuator is located at position 2. The PZT actuator is excited by random white noise from the built-in signal generator in BK3550. The random signal with the RMS value of 1 volt is amplified 90 times through the SQV3/500, the three-channel voltage transformer. The PVDF films are equally spaced and distributed over the beam as shown in Figure 2. Both the actuator and sensor signals are weighted by Hanning window to reduce the leakage. The FRF measurements are performed by roving the PVDF sensors with the fixed PZT actuator. Therefore, seven sets of FRFs can be obtained. Through the IEEE-488 interface, the measured data is transferred to the personal computer that is equipped with CADA-PC, a general purpose curve-fitter. By the operation on the sets of FRFs in CADA-PC, the modal parameters, including natural frequencies, damping ratios and mode shapes can be extracted. It is noted that since the FRF as derived and shown in Equation (4) is identical to the conventional modal format of FRF. The conventional curve-fitting algorithm is suitable for determining the modal parameters. In particular, the extracted mode shapes are the mode shapes of the slope differences between the two edges of the PVDF films. This will be further discussed in the next section.

RESULTS AND DISCUSSIONS

The physical properties of beam, PZT and PVDF patches are shown in Tables 1-3 respectively. The theoretical natural frequencies and mode shapes can be determined through Equations (1) and (2). By assuming the modal damping ratios to be 0.01, one can obtain the theoretical FRF from Equation (4). In the following discussions, the theoretical, measured and synthesized FRFs are compared. The modal parameters determined from the curve-fitting process will also be evaluated.

Verification of FRFs

Figures 4(a) and 4(b) show two typical FRFs respectively. Figure 4(a) shows the point FRF for i=2, j=2 that the sensing point is the same as the actuation one. There are antiresonance points between resonances. The shapes of FRF curves agree each other well, although the amplitude of the theoretical FRF is different from that of the experimental one. The synthesized FRF that is the regenerated FRF by the use of the extracted modal parameters.The agreement between the

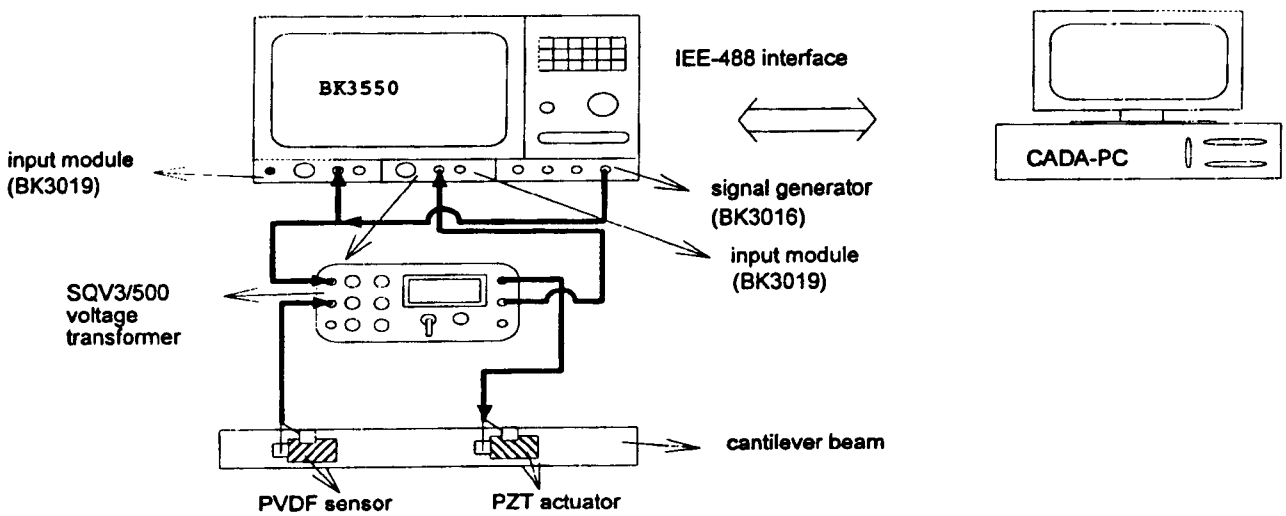

Figure 3. Experimental Setup

experimental and synthesized FRFs indicates the acceptance of curve-fitting algorithms.

Figure 4(b) shows the transfer FRF for i=14, j=2 that the sensing point is far away from the actuation one. There is a peak at 60 Hz due to the electronic noise. The synthesized FRF agrees well with the experimental one and also eliminates the 60 Hz noise. The FRF comparison is quite well for their shapes. The difference in amplitude between the theoretical and experimental results may come from the improper scale of voltage transformer.

Figures 5(a) and 5(b) shows the coherence functions corresponding to Figure 4(a) and 4(b). In general, the coherence value to be above 0.8 indicates the reliability of the experiments. The low coherence values at low frequency range in Figure 5(b) are due to the small dynamic range. The theoretical FRF shows over 120 dB dynamic ranges at low frequencies. The BK3550 has only about 80 dB dynamic range. In summary, the measured FRFs are applicable to further operation of the extraction of modal parameters.

Verification of Modal Parameters

Table 4 shows the comparison of natural frequencies between the theoretical and experimental results. Except the first natural frequency having -7.6% difference, others are within 5% difference

Table 1. Physical properties of cantilever beam

Material	Steel
length(L_b)	0.3(m)
width(b_b)	0.04(m)
thickness(t_b)	0.002(m)
density(ρ_b)	7870(kg/m^3)
Young's Modulus(E_b)	207×10^9(N/m^2)

Table 2. Physical properties of PZT patch

Type	PSI-5A-S2
length(l_c)	38 (mm)
width(b_c)	19 (mm)
thickness(t_c)	1.905 (mm)
Young's Modulus(E_c)	6.3×10^{10} (N/m^2)
density(ρ_c)	7650 (kg/m^3)
piezoelectric dielectric strain constant ($d_{31}=d_{32}$)	166×10^{-12} (m/V)

Table 3. Physical properties of PVDF film

Type	SDT1-028K
length(l_p)	38 (mm)
width(b_p)	19 (mm)
thickness(tp)	28×10^{-6} (m)
Young's Modulus(E_p)	2×10^9 (N/m^2)
density(ρ_p)	1800 (kg/m^3)
piezoelectric field intensity constant ($e_{31}=e_{32}$)	54×10^{-3} (m/V)
permittivity(ε)	106×10^{-12} (F/m)

Table 4. Comparison of natural frequencies

mode	exp. results (Hz)	Theo. Results (Hz)	error percentage (%)
$f_{1,1}$	17.00	18.411	-7.664
$f_{2,1}$	110.46	115.377	-4.262
$f_{1,2}$	307.00	323.058	-4.971
$f_{2,2}$	602.73	633.064	-4.792

Table 5. Modal damping ratios of the beam

mode	damping ratio (%)
$\xi_{1,1}$	3.23
$\xi_{2,1}$	1.00
$\xi_{1,2}$	0.39
$\xi_{2,2}$	0.30

The gradual shift of natural frequencies may be caused by the improper material stiffness and can be easily adjusted.

In theoretical analysis, the structural damping ratios can not be obtained and so forth assumed to be 0.01 for generating the FRFs. The modal damping ratios can be extracted through the curve-fitting process and shown in Table 5. The first modal damping ratio is slightly higher. This may be due to the insufficient dynamic range or the inaccurate peak value of resonance. The applications of PZT actuator and PVDF sensors may also contribute to increase the structure damping effect. Nevertheless, the extracted modal damping ratios generally agree with steel materials.

This work is to determine the modal parameters of the first four interested modes. It should be noted that the FRF measurement is performed by the fixed PZT actuator and the roving PVDF sensor. Therefore, the PVDF mode shape function can be extracted through the curve-fitting process. Both the experimental and theoretical mode shapes that are the slope difference between the two edges of PVDFsensors are shown in Figures 6(a) and 6(b) respectively. One can observe that both mode shapes agree well. The PVDF slope sensor mode shapes appear as the mirror image of displacement mode shape against the clamped end [11]. To further examine the correctness of the extracted mode shapes. Both the MSF (modal scale factor) and MAC (modal assurance criterion) [12] that are the indicator for the evaluation of similarity between two mode shapes. Tables 6 and 7 show the MSF and MAC matrix for the comparison between the experimental and theoretical mode shapes. That the diagonal terms of the MSF and MAC matrices approach to one represents the perfect agreement between the two mode shapes. When the off-diagonal terms of the MSF and MAC matrices are close to zero, the two mode shapes possess the perfect orthogonality. One can observe that both experimental and theoretical mode shapes have certain degree of similarity and possess the orthognality of mode shapes.

CONCLUSIONS

This paper experimentally verifies the use of PZT actuators and

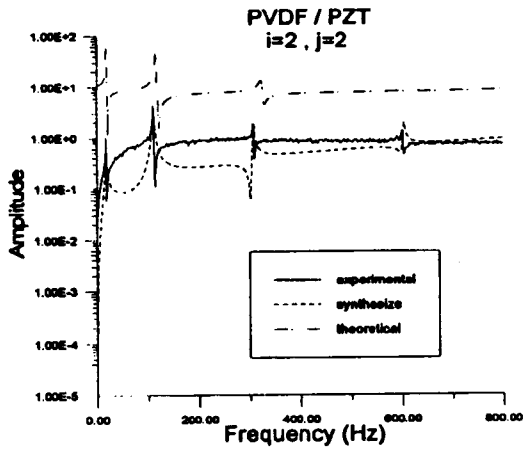

(a)i=2, j=2

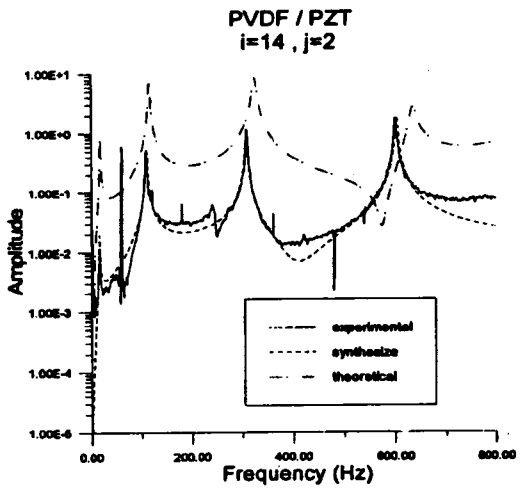

(b) i=14, j=2

Figure 4. Frequency response functions

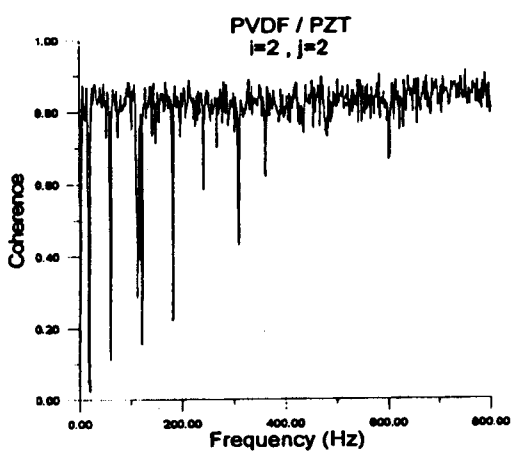

(a)i=2, j=2

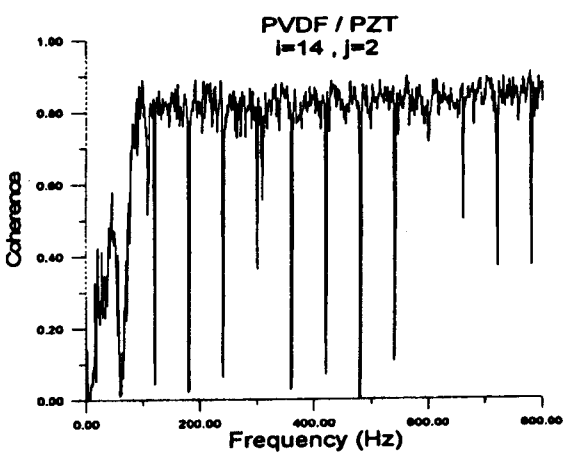

(b) i=14, j=2

Figure 5. Coherence functions

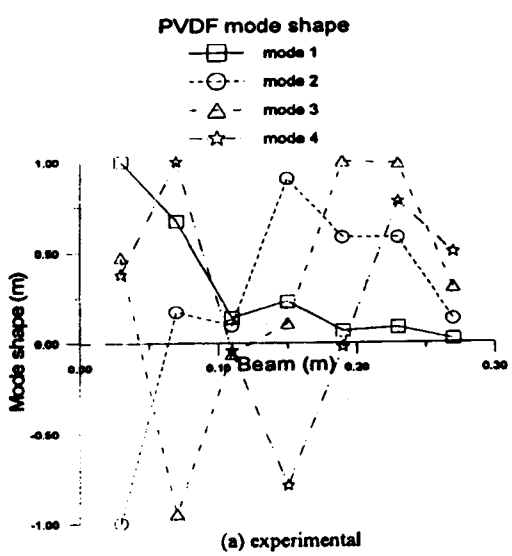

(a) experimental

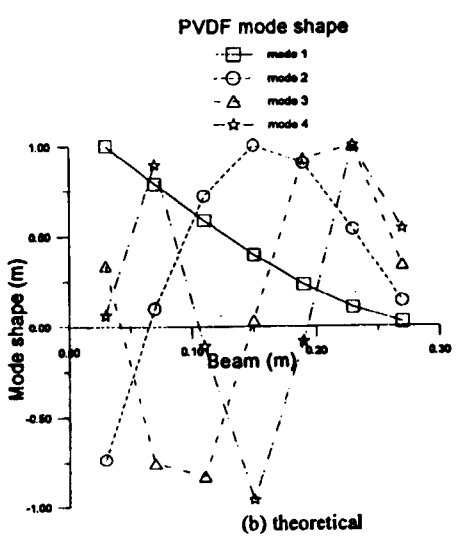

(b) theoretical

Figure 6. The first four PVDF mode shapes

Table 6. MSF matrix for experimental and theoretical PVDF mode shapes

mode	1	2	3	4
1	**0.8247-i0.2353**	-0.2286-i0.1316	-0.0168+i0.1258	0.2761-i0.0825
2	0.124+i0.0633	**-0.8857+i0.1071**	-0.2172+i0.0209	0.0745-i0.0335
3	-0.0187+i0.3085	0.3903-i0.1575	**0.7889-i0.2472**	0.0465-i0.0059
4	0.1888+i0.109	-0.041-i0.1617	0.0369+i0.1083	**0.9177+i0.2119**

Table 7. MAC matrix for experimental and theoretical PVDF mode shapes

mode	1	2	3	4
1	**0.6801**	0.0523	0.0003	0.0762
2	0.0154	**0.7845**	0.0472	0.0055
3	0.0003	0.1523	**0.6224**	0.0022
4	0.0357	0.0017	0.0014	**0.8422**

PVDF sensors for structural modal testing. The system modal arameters, including natural frequencies, damping ratios and mode shapes are properly identified. In particular, the extracted mode shapes are physically interpreted as the slope difference between two edges of the PVDF sensors. The FRFs between the PZT actuator and PVDF sensors can also be derived and expressed in conventional modal format. Theconventional modal parameter extraction methods can be suitable to determine the modal parameters for the piezoceramic structures. The system information is properly provided and can be adopted for control application. The idea of smart structure testing (SST) can also be enhanced.

ACKNOWLEDGMENT

The authors gratefully thank National Science Council for the support of this work under the grant of NSC87-2122-E-020-003.

REFERENCE

1. Crawley, E.F. and de Luis, J., 1987, "Use of Piezoelectric Actuators as Elements of Intelligent Structures," *AIAA Journal*, Vol. 25, pp. 1373-1385.
2. Bailey, T. and Hubbard, J.E., 1986, "Distributed Piezoelectric-Polymer Active Vibration Control of a Cantilevered Beam," *Journal of Guidance Control*, Vol. 6, pp. 605-611.
3. Wang, B.T. and Rogers, C.A., 1991, "Modeling of Finite-Length Spatially Distributed Induced Strain Actuators for Laminate Beams Structures," *Journal of Intelligent Material Systems and Structures*, Vol. 2, pp. 38-58.
4. Dimitriadis, E.K., Fuller, C.R. and Rogers, C.A., 1991, "Piezoelectric Actuators for Distributed Vibration Excitation of Thin Plate," *Journal of Vibration and Acoustics*, Vol.113, pp. 100-107.
5. Wang, B.T. and Rogers, C.A., 1991, "Laminate Plate Theory for Spatially Distributed Induced Strain Actuators," *Journal of Composite Materials*, Vol. 25, pp. 433-452.
6. Gibbs, G.P. and Fuller, C.R., 1992, "Excitation of Thin Beams Using Asymmetric Piezoelectric Actuators," *Journal of Acoustical Society of America*, Vol. 92, pp. 3221-3227.
7. Hubbard, J.E., 1987, "Distributed Sensors and Actuators for Vibration Control in Elastic Components," *Noise-Con 87*, pp. 407-412.
8. Clark, R.L. and Fuller, C.R., 1992, "Modal Sensing of Efficient Acoustic Radiators with PVDF Distributed Sensors in Active Structural Acoustic Approaches," *Journal of Acoustical Society of America*, Vol. 91, pp. 3321-3329.
9. Lee, C.K. and Moon, F.C., 1990, "Modal Sensors/Actuators," *Journal of Applied Mechanics*, Vol. 57, pp. 434-441.
10. Clark, R.L., Burdisso, R.A. and Fuller, C.R., 1993, "Design Approaches for Shaping Polyvinylidene Fluoride Sensors in Active Structural Acoustic Control (ASAC)," *Journal of Intelligent Material Systems and Structures*, Vol. 4, pp. 354-365.
11. Wang, B. T., Wang, C.C., 1997, "Feasibility Analysis of Using Piezoceramic Transducers for Cantilever Beam Modal Testing," *Smart Materials and Structures*, Vol. 6, pp. 106-116.
12. Ewins, D.J., 1986, *Modal Testing: Theory and Practice*, Research Studies Press Ltd., Letchworth, Hertfordshire, England.

壓電材料樑之系統辨識

陳榮亮
王柏村

國立屏東科技大學機械工程技術系

摘要

本文探討利用壓電片驅動器和壓電薄膜感測器進行系統辨識之技術，將一有限長度的壓電薄膜陣列平均的分佈在懸臂樑上當感測器，將兩有限長度的壓電片對稱的結合在樑之兩側並做180度相位角差之激振，使其爲純彎矩激振。以模態分析之理論基礎推導對於壓電材料樑系統之傳統模態形式的頻率響應函數，並分別驗證得到壓電片和壓電薄膜模態振型之物理意義。由實驗量測可以得到壓電片驅動器和壓電薄膜感測器間的頻率響應函數，由一系列的頻率響應函數可求得模態參數，包括系統之自然頻率、模態振型及阻尼比，從實驗分析證明與理論推衍之結果相當吻合，成功的完成系統辨識，由此系統的模態參數可進一步應用到控制及結構破壞診斷。